Automated vision-based inspection of mould and part quality in soft tooling injection moulding using imaging and deep learning

Zhang, Yang; Shan, Shuo; Frumosu, Flavia D.; Calaon, Matteo; Yang, Wenzhen; Liu, Yu; Hansen, Hans N.

Published in:
C I R P Annals

Link to article, DOI:
10.1016/j.cirp.2022.04.022

Publication date:
2022

Document Version
Publisher's PDF, also known as Version of record

CIRP Annals - Manufacturing Technology 71 (2022) 429–432

Contents lists available at ScienceDirect

CIRP Annals - Manufacturing Technology

journal homepage: https://www.editorialmanager.com/CIRP/default.aspx

Automated vision-based inspection of mould and part quality in soft tooling injection moulding using imaging and deep learning

Yang Zhang[a,*], Shuo Shan[a], Flavia D. Frumosu[b], Matteo Calaon[a], Wenzhen Yang[c], Yu Liu[c], Hans N. Hansen (1)[a]

[a] Department of Mechanical Engineering, Technical University of Denmark, Kgs. Lyngby, Denmark
[b] Department of Applied Mathematics and Computer Science, Technical University of Denmark, Kgs. Lyngby, Denmark
[c] School of Mechanical Engineering, Jiangnan University, Wuxi, Jiangsu, China

ARTICLE INFO

Article history:
Available online 6 May 2022

Keywords:
Digital manufacturing system
In-process measurement
Injection moulding

ABSTRACT

Automated real time quality monitoring is one of the key enablers for future high-speed production. In this research, an in-process monitoring procedure based on computer vision inspection and deep learning is proposed to indicate the tool and part quality during soft tooling injection moulding. Multiple types of injection moulding defects can be detected by the proposed method. Geometrical dimensions of the part can be measured simultaneously and the uncertainty can be quantified. Based on the obtained data, automated quality evaluation can be achieved in-process and a decision signal can be sent back to the injection moulding system for process adjustment.

1. Introduction

Automation is becoming more and more important in today's manufacturing sector. The research problem addressed is how to monitor mould and part quality in-process during injection moulding (IM). With the development of computing hardware and software, especially in the fields of image processing technologies, computer vision techniques for automatic tracking of tool condition started to be largely adopted in manufacturing [1]. Soft tooling is a cost-effective method of tooling for injection moulding [2]. Instead of using the conventional metal tools, moulds produced by polymer additive manufacturing, especially vat photopolymerization, are used in injection moulding.

The soft tooling process chain consists of two major process steps, i.e., additive manufacturing of a soft tool followed by injection moulding [2]. A pair of moulds produced by vat photopolymerization can last up to 1000 cycles in a typical injection moulding process [3]. This process is suitable for prototype productions and pilot productions due to improved geometrical freedom, short lead time and low cost. However, it is a challenge to predict the life of the tool (mould) due to the complexity of the part. Compared to metal tools, the soft tool has a much shorter lifetime. It is extremely easy to break thin walls due to high injection pressures. Additionally, the parts suffer from potentially higher deformations during ejection due to the heat accumulation on the mould. Traditional monitoring like temperature and pressure sensors are not sufficient to indicate the status of the mould. Effective monitoring procedures require a continuous and iterative mechanism to keep evaluating the status of the mould. The calculated decision signal is then fed back to the injection moulding process for stopping or adjusting the moulding parameters. Installation of new sensors, data analysis, and decision-making based on the acquired data will be demanded for the future manufacturing systems [4].

Computers' development allows faster computation, and it is now possible to run complex neural network models along with high-speed mass production. Misaka et al. [5] successfully applied deep learning in a turning process to correlate machining quality with simulation. In the mass production of micro parts, reliable in-process measurements are challenged by high speed, limited space, varied temperature and other noise. Computer vision based on image capturing and analysis has advantages in speed, stability, accuracy and maintenance [6]. Tada and Ishibe [7] has reported an automatic inspection using image processing for monitoring silver streaks during injection moulding. The work presented the possibility to extract the silver streaks based on a grey scales detection procedure. However, other typical defects such as flash were not distinguished. Bai et al. [8] described a machine vision system, which can potentially identify different defects by comparing images of conformed parts with deceptive ones. Yet only one type of IM failure (underfilled parts) was reported in their work. Wei et al. [9] presented their online dimensional measurement system for microparts, based on charged-coupled device (CCD) camera with optical fibre. However, their method relies on a high contrast between the part and the background. Otherwise, the image analysis method is not able to extract the contour of the part.

This research aims for a solution to monitor the product and mould quality in-process and to collect data in order to achieve a decision if the IM process needs to be optimized. A computer vision system that consists of a CCD camera and a thermal camera was installed. A two-branch deep learning (neural network) model based on image segmentation and bounding box detection has been used.

The image segmentation branch was employed to analyse obtained images and output detection of possible failures while the bounding box detection was employed to determine the dimension of the parts. For the first time, the uncertainty of dimensional

* Corresponding author.
E-mail address: yazh@mek.dtu.dk (Y. Zhang).

https://doi.org/10.1016/j.cirp.2022.04.022

measurement based on machine learning is estimated. Moreover, the accuracy of the failure detection was evaluated.

2. Experimental setup

The demonstrating part for the injection moulding was a thin wall case with a size of 25 × 13 mm approximately.

In order to increase the variability of the data and the robustness of the trained model, different colours of moulds were printed via a self-developed DLP printers [10]. FunToDo Industrial Blend resin in black or red colour was mixed with Formlabs® Rigid 10 K in different ratios to improve mechanical properties as a mould and obtain black, white, pink, and red moulds. Transparent moulds were printed using resin from 3Dresyns.

Injection moulding tests were conducted on a BOY XS from Dr. Boy GmbH & Co. ABS Terluran GP-35 in nature colour was used as injection material. To generate a variety of defects on the mould and parts, a full factorial DOE with 2 factors and 3 levels was carried out (Table 1) for each pair of moulds. 5 cycles were conducted for each run. 3 repetitions were conducted using a new mould for each colour. Mould breakage, underfilling, and flashes were observed by the operator after the injection moulding tests were performed.

Table 1
DOE for injection moulding used to generate varied data.

Packing Pressure (Bars)	0	200	400
Melt T (°C)	200	220	240

A camera (BFS-U3−31S4C, FLIR) with lens (HF25HA-1B, FIJIFILM) was mounted on the top of the stationary side of the mould (Fig. 1). Two images were captured in each cycle: first one before part ejection; the second one on the mould after part ejection. A thermal camera (Optris OPTPI64IT900) was used to measure the temperature on the part simultaneously when the CCD image was captured.

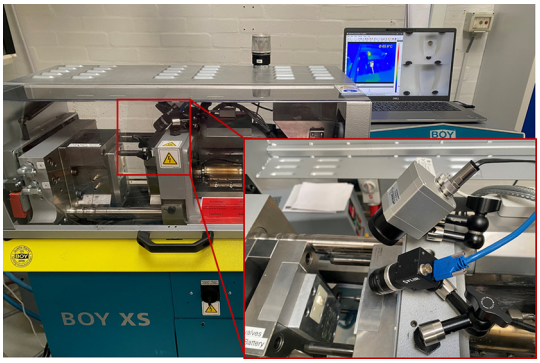

Fig. 1. Both CCD and thermal cameras were installed on the stationary side of the mould. The thermal camera measured the temperature of the part when the CCD camera captured the image.

In order to have a demonstrating area to conduct dimensional measurements, a protruding rectangle, so-called “Dimensional Measurement (DM) area” was designed (approximately 2 × 3 mm) in the centre of the part. This DM area can be captured by the CCD camera. Subsequently to the acquisition, the length and the width are used for evaluating the dimensional measurements by using a deep learning model. To verify the reliability of the model measurements output, a DeMeet 220 3D Coordinate Measuring Machine (CMM) was used to perform physical measurements on selected samples.

3. Methodology for defects detection and dimension measurements

3.1. Two-branch neural network for defects detection and dimension measuring

The raw images captured from the CCD camera were first pre-processed (cropping and concatenating), then they were fed into two

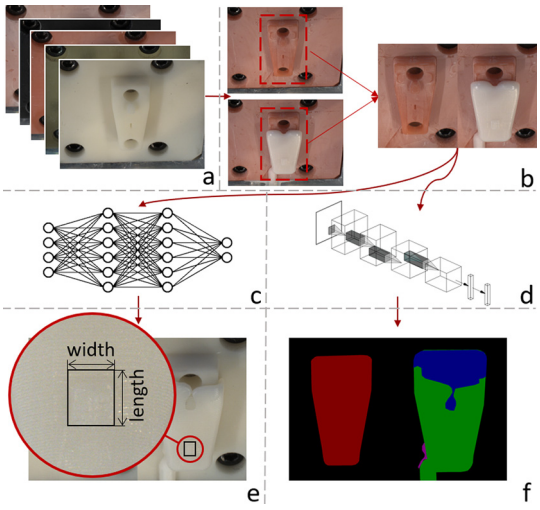

Fig. 2. Two-branch neural network: a. raw images from the CCD camera; b. images are pre-processed. Example is a red mould and an underfilled part; c. DM branch for dimensional measurement; d. Sem-seg branch for segmentation; e. DM branch outputs dimensions of a bounding box for the DM area; f. Sem-seg branch outputs segmentation indicating possible defects.

seperated neural networks, i.e. Semantic segmentation (Sem-seg) branch for defect labelling and Dimensional measurement (DM) branch for DM area labelling, as illustrated in Fig. 2.

Sem-seg branch consists of a neural network called DeepLab version 3 [11,12]. When the images are fed into this branch, each pixel in the image will be classified with a specified class. The output (an image with the same size as the input image) consists of several semantic segments, which indicates different types of defects in injection moulding.

DM branch focuses on detecting and measuring the DM area on the pre-processed images. It will output the length and width information of the bounding box on the DM area. The employed neural network is YOLO [13] version 5.

3.2. Data preparation and dataset generation

In order to prepare images for the Sem-seg branch training, 5 classes were manually annotated on the images: core, part, mould breakage, underfilling and flash. The annotation depends on the selected points used by the operator for marking a specific class. This process was carried out on LabelMe [14].

- Core: the mould on the movable side. Annotated in red.
- Mould Breakage: parts of the mould may break during injection moulding. It is a typical defect when soft tooling is used. Once this type of defect occurs, the IM process needs to be terminated and the mould needs to be changed. Annotated in yellow.
- Part: the injection moulded part. Annotated in green.

Underfilling: it happens when the mould cavity is not fully filled and as a result, the obtained part is shorter. Once this type of defect occurs, the part is faulty, and the parameters of IM need to be optimized. Annotated in blue.

- Flash: flash is excess plastic that forms on the surface of injection moulded parts. Once this type of defect occurs, the part is faulty, and the parameters of IM need to be optimized. Annotated in pink.
- Background: the pixels that are not classified are automatically labelled as the background class. Annotated in black.

Fig. 3 shows the annotation on pre-processed images. On the transparent mould, annotation for mould breakage and the underfilled part was visualized; on the pink mould, annotation for mould breakage and flash was visualized.

For the DM branch training, a bounding box on the DM area is labelled on every image, illustrated in Fig. 3 as well.

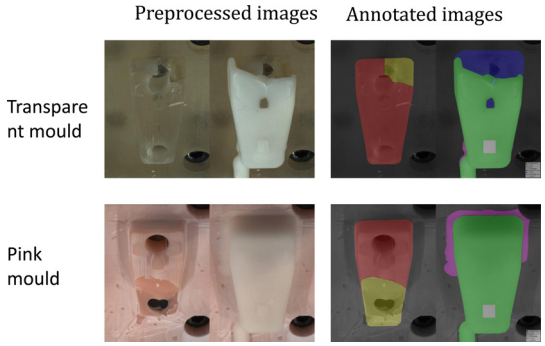

Fig. 3. Images are annotated to prepare dataset for neural network training.

4. Results and evaluation

The training is conducted via PyTorch and NVIDIA® TESLA V100. 300 labelled images were used as a training set. Data augmentation techniques like cropping, flipping, rotating, scaling, random erasing and gaussian blur [15] were also performed during training. For the Sem-seg branch, 45 labelled images were used for testing. For the DM branch, 180 images were tested and compared with CMM measurements.

4.1. Evaluation of the Sem-seg results

Fig. 4 shows the detection of classes for 2 types of moulds. All the defined injection moulding defects are detected here: mould breakage on the black mould, flash on the part, and underfilling on the part. These results demonstrate that the proposed method can detect and segment the defined classes.

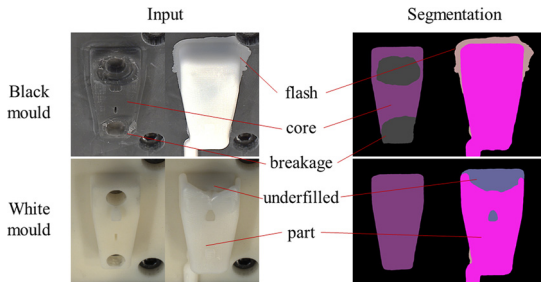

Fig. 4. Defects detection by the trained neural network.

Two indices, Recall and Intersection over Union (IoU), were used to evaluate the segmentation models. The pixels are classified into categories: True Positive (TP) represents the number of pixels that are correctly predicted in the given class; False Positive (FP) represents the number of pixels that are predicted wrongly as the given class; False Negative (FN) represents the number of pixels that are predicted wrongly as the given non-class [16].

Recall: represents the ratio of the correctly predicted pixels to the number of labelled pixels of a specific class (Eq. (1)). It describes the completeness of the positive detection relative to the object:

$$recall = \frac{TP}{TP + FN} \tag{1}$$

IoU: measures the number of pixels common between the target and detections divided by the total number of pixels present in both, as calculated by Eq. (2). It quantifies the percent overlap between the target and the detection:

$$IoU = \frac{TP}{TP + FN + FP} \tag{2}$$

The recall and IoU of segmentation are shown in Fig. 5. The obtained results indicate that the classes are identified correctly to a large extent as it can also be visualized in Fig. 4. For a detection purpose this result indicates that the proposed method is able to retrieve the defined defects and can be applied in production.

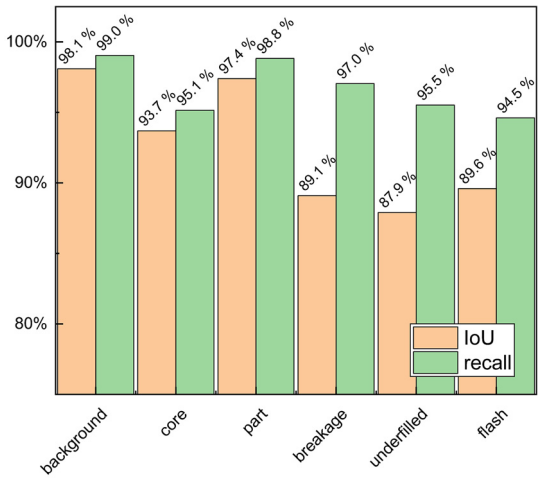

Fig. 5. Evaluation of segmentation by "Recall" and "IoU".

4.2. Evaluation of the DM branch

The DM branch directly outputs the pixel numbers for the width and length of the bounding box. A scaling coefficient, S, was applied in order to find out the corresponding dimension for a pixel. One sample was measured using the CMM 15 times. The image corresponding to the sample was fed into the neural network 15 times and piexel numbers for width and length was obtained. S was calculated by Eq. (3) for the width and length separately. For the width, 1 pixel corresponds to 19 µm and for the length, 1 pixel corresponds to 26 µm.

$$S = \frac{Average\ Dimension}{Average\ Pixel\ number} \tag{3}$$

The temperature of the part when the image was captured was around 40–60 °C. This means that the actual size that is captured by camera is larger than when it is measured by the CMM due to material shrinkage. The coefficient of linear thermal expansion, α, has a value of 0,8 $*10^{-4}$ m/ (m °C) for the injection moulding material. In this way, the output dimension, $D_{20^\circ C,}$ will be calculated by Eq. (4):

$$D_{20^\circ C=} Pixel * S * (1 - \alpha * \Delta T) \tag{4}$$

The uncertainty of the CMM measurements was investigated according to the "Guide to the expression of uncertainty in measurement" (GUM) [17]. Machine (u_m), process (u_p) and environment (u_e) errors were taken into account. u_m is calculated according to Eq. (5), where the maximum permissible error (MPE) of the equipment is 2.5 µm. 15 repetitive measurements were conducted on one sample in order to estimate u_p. Eq. (6) was used to calculate u_p, where the standard deviation (std) is 0.006 µm and 0.009 µm for the width and length respectively. u_e was estimated by Eq.(7), where ΔT is the temperature range during measurement (± 1 °C), D is the dimension that is measured, α is the thermal expansion coefficient, and 0.7 is the applied distribution factor. Hereby, the combined uncertainty, U_{CMM} in Eq. (8) for CMM measurements, is 4.4 µm for both the width and length measurements, where k is 2 for the 95% confidence level,

$$u_m = 0.6 \times MPE \tag{5}$$

$$u_p = std/\sqrt{15} \tag{6}$$

$$u_e = \Delta T \times \alpha \times D \times 0.7 \tag{7}$$

$$U_{CMM} = k\sqrt{u_m^2 + u_p^2 + u_e^2} \tag{8}$$

The precision of the neural network was evaluated following the GUM approach as well. 2 uncertainty contributors u_c and u_p are taken into consideration. $u_{c,}$ is the uncertainty for the camera, including the contribution from the camera and the capturing environment (for instance, the lightning condition). u_p is the uncertainty for the neural

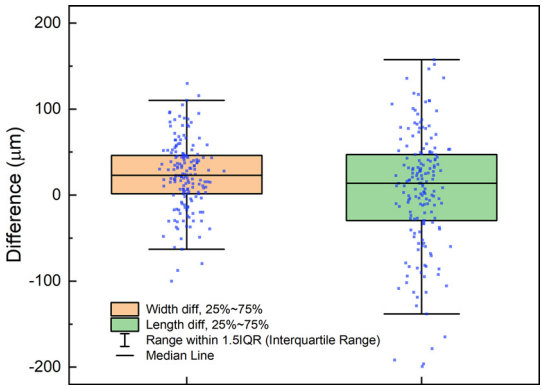

Fig. 6. Difference between the neural network output and CMM measurements. Data points are jittered around the boxplots. The box shows 25%–75% (i.e. interquartile range) of the data, the middle line shows the median value of the dataset.

network processing, including the contribution from the operators, and the network generation. In this context, the operators are defined as the persons who annotated the images.

To obtain u_c, 25 images were captured on the same part at 60 °C ± 1 °C, and the lightning was varied during the image capturing. These 25 images were fed into a trained neural network and the number of pixels for the width and length were obtained. The standard deviation was used to calculate u_c for width and length separately by Eq. (9).

In order to obtain u_p, the training dataset (300 images), which were annotated by 3 operators, were fed into the DM branch 20 times. This process generated 20 models with different estimated parameters due to the training. One identical image was processed by each of these 20 models, then pixel numbers for the width and length number were obtained as inference from each model. The standard deviation of the number of pixels was used for calculating u_p according to Eq. (10), for the width and length separately. Finally, the combined uncertainty, $U_{network}$ for the neural network inference was calculated by Eq. (11), where k is 2 for the 95% confidence level.

$$u_c = std/\sqrt{25} \tag{9}$$

$$u_p = std/\sqrt{20} \tag{10}$$

$$U_{network} = k\sqrt{u_c^2 + u_p^2} \tag{11}$$

In this way, the pixel uncertainty is computed from the neural network inference. For the width, the uncertainty is 1.62 pixels and for the length it is 1.58 pixels. By applying the scaling coefficient and thermal expansion coefficient (Eq. (4)), the uncertainty corresponds to 30 µm and 41 µm for the width and length correspondingly.

The output dimensions for the validation groups (180 images) obtained from the trained neural network were compared with the CMM measurements on the corresponding parts. The differences, calculated by subtracting the DM output from the CMM measurements, are plotted in Fig. 6 via boxplots. For the width measurements, middle 50% of the samples lie within the difference range from 1 µm to 46 µm; for the length measurements, middle 50% of the samples lie within the range −29 µm to 47 µm. This distribution range aligns with the uncertainty estimation. If the absolute difference is standardized by dividing the CMM measurement value, in average, a 1.8% (width) and 1.9% (length) difference exists between the neural network output and the CMM measurements. The difference observed between the width and length can be explained by the bounding box annotation. In Fig. 2, the length is more difficult to quantify visually due to the shadow that appears due to the camera tilting. Naturally, this will interfere with the annotation process that will also affect the training of the neural network model.

5. Conclusion

In this research, a novel automatic monitoring framework for soft tooling IM is proposed. Through image segmentation and bounding box detection, defects identification and dimensional information can be obtained. The accuracy of defect detection was evaluated, and it showed that the proposed method has good capability to retrieve the defined defects in injection moulding. It means that data can be streamed to the IM machine and other remote subscribers for further decision making. The dimensions of the part or mould can be measured simultaneously during injection moulding. The neural network was also used to establish an estimate of the dimensions and corresponding uncertainties. The measurement uncertainty for the applied neural network is 30 µm for width and 41 µm for length. The uncertainty will be reduced in future work by improving the camera resolution, calibration and the accuracy of manual annotating. Image augmentation will be applied in the future in order to improve the efficiency and transferability of the training. Mould variation will be applied to the training in order to enhance the model's robustness.

Declaration of Competing Interest

The authors declare that they have no known competing financial interests or personal relationships that could have appeared to influence the work reported in this paper.

Acknowledgements

The work has been supported by Innovation Fund Denmark through the project "Research based enterprise-qualification and enterprising of soft tooling" (Grant No. 8057–00031).

References

[1] Wiederkehr P, Finkeldey F, Merhofe T (2021) Augmented Semantic Segmentation for the Digitization of Grinding Tools Based on Deep Learning. *CIRP Annals* 70/1:297–300.
[2] Zhang Y, Pedersen DP, Gøtje AS, Mischkot M (2017) A Soft Tooling Process Chain Employing Additive Manufacturing for Injection Molding of a 3D Component with Micro Pillars. *Journal of Manufacturing Processes* 27:138–144.
[3] Hofstätter T, Mischkot M, Pedersen DB, Tosello G, Hansen HN (2016) Evolution of Surface Texture and Cracks During Injection Molding of Fiber-Reinforced, Additively-Manufactured, Injection Molding Inserts. In: *Proceedings of the ASPE Summer Topical Meeting 2016: Dimensional Accuracy and Surface Finish in Additive Manufacturing.*
[4] ElMaraghy H, Monostori L, Schuh G, ElMaraghy W (2021) Evolution and Future of Manufacturing Systems. *CIRP Annals* 70/2:635–658.
[5] Misaka T, Herwan J, Ogura I, Furukawa Y (2021) Turning Process Monitoring with Deep Neural Network Trained by FEM Simulation. *Procedia CIRP* 104:376–380.
[6] Cheng, KO, Lawa, NF, Siua,WC, 2010, Fast Extraction of Wavelet-Based Features from JPEG Images for Joint Retrieval with JPEG2000 Images, Pattern Recognition, v43, n10, 3314–3323,
[7] Tada Y, Ishibe N (1994) Automatic Inspection of Injection Moldings (in the Case of Silver Streaks). In: *Proceedings of the Japan-U.S.A. Symposium on Flexible Automation - a Pacific Rim Conference*, 1057–1060.
[8] Fan B, Zheng H, Wang Y, Wang C, Liao S (2016) Research on Machine Vision System of Monitoring Injection Molding Processing. In: *Proceedings of the SPIE 9903, Seventh International Symposium on Precision Mechanical Measurements*, 99030R.
[9] Wei X, Li J, Liu X, Zhao S (2014) A Fast on-line two-Dimensional Sizes Measurement Method for Micro Part. *Computer Modeling & New Technologies* 18/2:52–56.
[10] Ribo MM (2020) *Vat Photopolymerization Process Chain*, Technical University of DenmarkKgs. Lyngby.
[11] Chen LC, Papandreou G, Kokkinos I, Murphy K, Yuille AL (2017) Deeplab: Semantic Image Segmentation with Deep Convolutional Nets, Atrous Convolution, and Fully Connected Crfs. *IEEE Transactions on Pattern Analysis And Machine Intelligence*, 40(4):834–848.
[12] Chen LC, Zhu Y, Papandreou G, Adam H (2018) Encoder-Decoder with Atrous Separable Convolution for Semantic Image Segmentation. In: *Proceedings of the European Conference on Computer Vision (ECCV)*, 801–818.
[13] Francies ML, Ata MM, Mohamed MA (2022) A Robust Multiclass 3D Object Recognition Based on Modern YOLO Deep Learning Algorithms. *Concurrency and Computation Practice and Experience* 34(1):e6517.
[14] Russell BC, Torralba A, Murphy KP, Freeman WT (2008) LabelMe: A Database and Web-Based Tool for Image Annotation. *International Journal of Computer Vision* 77(1–3):157–173.
[15] Shorten C, Khoshgoftaar TM (2019) A survey on Image Data Augmentation for Deep Learning. *Journal of Big Data* 6(1):60.
[16] Fernandez-Moral E, Martins R, Wolf D, Rives P (2018) A New Metric for Evaluating Semantic Segmentation: Leveraging Global and Contour Accuracy. In: *Proceedings of the IEEE Intelligent Vehicles Symposium (IV)*, 1051–1056.
[17] ISO/IEC GUIDE 98-3:2008 Uncertainty of measurement — Part 3: Guide to the expression of uncertainty in measurement (GUM:1995)